Journal of Fluorescence, Vol. 1, No. 4, 1991

Distance Distributions Recovered from Steady-State Fluorescence Measurements on Thirteen Donor–Acceptor Pairs with Different Förster Distances

Wieslaw Wiczk,[1,3] Peggy S. Eis,[1] Mayer N. Fishman,[1] Michael L. Johnson,[2] and Joseph R. Lakowicz[1,4]

Received November 15, 1990; revised August 16, 1991; accepted August 16, 1991

The end-to-end distance distribution of a flexible molecule was recovered from steady-state fluorescence energy transfer measurements using the method suggested by Cantor and Pechukas (*Proc. Natl. Acad. Sci. USA* **68**, 2099–2101, 1971). In this method, the Förster distance (R_0) is varied by attaching different donor–acceptor (D–A) pairs to the flexible linker of interest. Distance distributions are then recovered from energy transfer efficiency measurements on the set of D–A pairs with different R_0 values. Thirteen D–A pair compounds were synthesized with R_0 values ranging from 6 to 32 Å. Each compound contained a tryptamine donor linked by an alkyl chain (~10 carbons) to 1 of 13 acceptors. Using these compounds, we have experimentally confirmed the Cantor and Pechukas method for recovering distance distributions. The measured transfer efficiencies, as a function of R_0, were fit to the transfer efficiencies predicted for both Gaussian and skewed Gaussian distance distributions. The data support the existence of a skewed Gaussian distribution, and we believe that this is the first experimental observation of an asymmetric distribution for a flexible molecule using fluorescence resonance energy transfer measurements. Finally, the experimentally recovered distance distribution was found to be in good agreement with the distribution predicted from the rotational isomeric state model of Flory (*Statistical Mechanics of Chain Molecules*, John Wiley & Sons, New York, 1969, Chaps. 1, 3, and 5) but not with the predicted distribution for a freely rotating or freely jointed chain.

KEY WORDS: Energy transfer; distance distributions; Förster distance; donor–acceptor pair; fluorescence spectroscopy; time-resolved fluorescence; frequency-domain fluorometry; fluorescence resonance energy transfer.

INTRODUCTION

The concept of recovering distance distributions from steady-state fluorescence energy transfer measurements was first proposed by Cantor and Pechukas [1]. Their method consists of labeling a molecule of interest with different donor–acceptor (D–A) pairs, thereby creating a set of molecules with different Förster (R_0) distances. One can then recover the distance distribution of the molecule by measuring the transfer efficiencies as a function of R_0. Due to the time and effort associated with the synthesis of many donor and acceptor labeled molecules, we previously developed an alternative method in which the R_0 is varied with a collisional quencher [3,4]. The distance distributions recovered using the col-

[1] University of Maryland, School of Medicine, Department of Biological Chemistry, 660 West Redwood Street, Baltimore, Maryland 21201.
[2] University of Virginia, Department of Pharmacology, Charlottesville, Virginia 22908.
[3] Permanent address: University of Gdańsk, Institute of Chemistry, Gdańsk 6, Sobieskiego 18, Poland.
[4] To whom correspondence should be addressed.

1053-0509/91/1200-0273$06.50/0

lisional quencher method are consistent with those that have been recovered using the time-resolved frequency-domain method [5–7] and by time-correlated single-photon counting [8]. A disadvantage of the quenching method is the limited range of R_0 values which can be obtained for reasonable amounts of quenching.

The Cantor and Pechukas method of using multiple D–A pairs (i.e., without quenching) has never, to our knowledge, been experimentally tested. Thus, we were interested in verifying this method and determining how it compares to the steady-state collisional quenching and time-resolved frequency-domain methods. If the Cantor and Pechukas method yields a similar distribution as compared to those recovered from the frequency-domain and steady-state quenching methods, then we can be more assured of the validity of the distance distribution recovered from all these methods. Additionally, it seemed possible that each D–A pair would sample a different part of the distance distribution and, thus, provide increased resolution of this distribution. Accordingly, we attempted to detect asymmetry in the distribution (i.e., skewness) and were successful in this attempt. Finally, we compared the recovered distribution with theoretical calculations using the rotational isomeric model [2].

THEORY

Energy Transfer

The efficiency of energy transfer, E, can be calculated from the relative intensities of the donor emission from the donor-alone control molecule (I_D) and of the donor emission from the D–A pair (I_{DA})

$$E = 1 - \frac{I_{DA}}{I_D} \tag{1}$$

For a donor and acceptor present at a fixed distance, r, this distance can be calculated from the energy transfer efficiency and the Förster distance using

$$E = \frac{R_0^6}{R_0^6 + r^6} \tag{2}$$

If a range of distances exists between the donor and the acceptor, then the apparent value of r from Eq. (2) represents a weighted average of the D–A distribution. The Förster distance can be calculated from the spectral properties of the chromophore

$$R_0^6 = \frac{9000\ (\ln 10)\ \kappa^2 \phi_D^0}{128\ \pi^5\ N n^4} \int_0^\infty F_D(\lambda)\ \epsilon_A(\lambda)\ \lambda^4\ d\lambda \tag{3}$$

where κ^2 is the orientation factor and is defined by

$$\kappa = \vec{D} \cdot \vec{A} - 3(\vec{D} \cdot \vec{R})(\vec{A} \cdot \vec{R}) \tag{4}$$

in which $\vec{D}$, $\vec{A}$, and $\vec{R}$ are unit vectors along the transition dipole directions of D and A and along the separation between D and A, respectively; ϕ_D^0 is the quantum yield of the donor in the absence of acceptor and quencher; n is the refractive index; N is Avogadro's number; $F_D(\lambda)$ is the emission spectrum of the donor with the area normalized to unity; $\epsilon_A(\lambda)$ is the absorption spectrum of the acceptor (M^{-1} cm^{-1}); and λ is the wavelength (nm).

Distance Distributions

If a D–A pair is connected by a flexible linker, then one expects a range of D–A distances. To recover the distribution of distances from steady-state measurements, one needs to measure E as the R_0 is varied by quenching [3,4] or to measure E for a number of D–A pairs with different R_0 values [1]. Since the data are not adequate to recover the distinct shape of this distribution, we parameterize the probability function assuming a Gaussian [$P_{Gau}(r)$] or a skewed Gaussian [$P_{sGau}(r)$] model. The Gaussian model probability distribution is defined here as

$$P_{Gau}(r) = \frac{1}{Z_{Gau}} \exp\left[-\frac{1}{2}\left(\frac{r - \bar{r}}{\sigma}\right)^2 \right] \tag{5}$$

where the normalization factor is

$$Z_{Gau} = \int_{r_{min}}^{r_{max}} \exp\left[-\frac{1}{2}\left(\frac{r - \bar{r}}{\sigma}\right)^2 \right] dr \tag{6}$$

for $r_{min} \le r \le r_{max}$; $P_{Gau}(r) = 0$ for $r < r_{min}$ and for $r > r_{max}$. The average distance and standard deviation of the untruncated Gaussian function are $\bar{r}$ and σ, respectively. The widths of the distributions are reported in terms of the half-width (full-width at half-maximum probability, hw). For a Gaussian, $hw = 2.354\sigma$. Our rationale for selecting this form for the distance distribution is given in the Appendix.

The skewed Gaussian model probability distribution is defined as a composite of two Gaussian functions,

for $r_{min} \leq r < r_m$,

$$P_{sGau}(r) = \frac{1}{Z_{sGau}} \exp\left[-\frac{1}{2}\left(\frac{r - r_m}{\sigma'_L}\right)^2 \right] \quad (7a)$$

for $r_m \leq r \leq r_{max}$,

$$P_{sGau}(r) = \frac{1}{Z_{sGau}} \exp\left[-\frac{1}{2}\left(\frac{r - r_m}{\sigma'_R}\right)^2 \right] \quad (7b)$$

where the normalization factor is

$$Z_{sGau} = \int_{r_{min}}^{r_m} \exp\left[-\frac{1}{2}\left(\frac{r - r_m}{\sigma'_L}\right)^2 \right] dr + \int_{r_m}^{r_{max}} \exp\left[-\frac{1}{2}\left(\frac{r - r_m}{\sigma'_R}\right)^2 \right] dr \quad (8)$$

and $P_{sGau}(r) = 0$ for $r < r_{min}$ and for $r > r_{max}$. The mode (most frequently occurring value of the distribution [9]) is r_m, $\sigma' = \frac{1}{2}(\sigma_L' + \sigma_R')$ is a parameter derived from the sum of the standard deviations of the Gaussians used for the left and right parts of the curve, and by analogy $hw = 2.354\sigma'$. The relative values of these standard deviations is described using the skew parameter (s):

$$\sigma_L' = 2\sigma'\left[\frac{1}{\exp(s) + 1}\right], \quad \text{for } r \leq r_m \quad (9a)$$

$$\sigma_R' = 2\sigma'\left[\frac{\exp(s)}{\exp(s) + 1}\right], \quad \text{for } r \geq r_m \quad (9b)$$

or alternatively,

$$\text{skew} = \ln\left(\frac{\sigma_R'}{\sigma_L'}\right) \quad (10)$$

The skew parameter (s) can vary from $-\infty$ to $+\infty$; for a nonskewed Gaussian curve $s = 0$. The skewed Gaussian model function and its derivative are continuous for $r_{min} < r < r_{max}$. According to these expressions, a skewed Gaussian with negative skew is wider on the side with $r < r_m$ and falls sharply on the side with $r > r_m$.

For an assumed distance distribution, $P(r)$, the efficiency of transfer can be calculated (c) using

$$E_{cR_0} = \int_{r=r_{min}}^{r_{max}} \frac{P(r)\, R_0^6}{R_0^6 + r^6} dr \quad (11)$$

where r_{min} and r_{max} are minimum and maximum distances for the calculation. To determine the distribution parameters from experimental data, the assumed distribution is varied to yield the minimum value of χ_R^2,

$$\chi_R^2 = \frac{1}{\nu} \sum_{R_0} \left(\frac{E_{R_0} - E_{cR_0}}{\Delta E} \right)^2 \quad (12)$$

where E_{R_0} are the measured efficiencies at each R_0 value, $\Delta E = 0.02$ is the estimated error in the measured efficiencies (E), and ν is the number of degrees of freedom.

Theoretical Histograms

The theoretical distance distribution histograms were generated by an implementation of the rotational isomeric state (RIS) model described by Flory [2,10]. In this model the conformation of each bond is restricted to one of several minimum energy conformations and the fractional population of each state is weighted by the Boltzmann energy. For example a carbon–carbon bond in an alkyl chain can have three orientations, *trans*, *gauche*$^+$, and *gauche*$^-$. The conformational space available to a chain-like molecule, such as the alkyl linker in these compounds, is simplified by fixing bond lengths and bond angles at their equilibrium values and allowing only a small number of rotational angles, which occur at energy minima. For an alkyl chain of n links, three positions are allowed for each bond (*trans*, *gauche*$^+$, and *gauche*$^-$), and the conformational space is represented as a set of 3^{n-1} distinct conformations. For each conformation two parameters may be defined, the end-to-end distance and the energy. This distance can be computed exactly using an explicit geometric calculation, whereas the probability is a function of the conformational energy, which must be estimated relative to the energies of other possible conformations.

To provide a basis for comparison of the results, the following three simpler models [2] were also implemented: (i) rotationally restricted (RR) but without energy weighting (like the RIS model, but all conformations have equal probability); (ii) freely rotating (FR), in which all bond rotational positions are equally likely; and (iii) freely jointed (FJ), in which all bond angles are equally likely as well. It was found that the distance distribution histograms based on the RR and FR models were indistinguishable for these compounds. In these simpler models all allowed conformations have equal probability so there is no need to estimate energies.

In the RIS model, the energy of a particular conformation is estimated as the sum of individual bond contributions; further, these energies are estimated to be

determined predominantly by only the position of the individual bond and its nearest-neighbor bonds. Once the energy has been estimated, the probability of conformation i [$P(c_i)$] is given by the Boltzmann probability for that energy divided by a normalization factor,

$$P(c_i) = \frac{1}{Z}\exp\left(\frac{-E(c_i)}{RT}\right) \quad (13)$$

where R is the universal gas constant, T is the absolute temperature, and Z, the normalization factor, is

$$Z = \sum_{\text{all } c_i} \exp\left(\frac{-E(c_i)}{RT}\right) \quad (14)$$

This energy rule and the distance computation together define a distance probability distribution function, $P(r)$. This distribution function could be calculated exactly using a complete enumeration of the conformations, but as a practical matter it was estimated using a histogram generated by picking a large number (e.g., 100,000) of random conformations, computing their distances and relative probabilities, and accumulating the results in the histogram. By comparison of separate, independent runs of this size, it was apparent that the shape of the distance distribution curve had converged to a stable shape (not shown in this paper); also, comparison of the histogram derived from a complete enumeration and similarly sized samples for smaller molecules indicated that this size gives a satisfactory level of convergence. Since the RIS conformational space for these alkyl molecules contains a large proportion of high-energy/low probability conformations, the efficiency of this random selection is markedly improved by using a Monte Carlo selection, in which the probability of selection of a particular conformation is proportional to its energy weighting [11,12]. For the simpler models, an ordinary random selection is sufficient because each conformation has equal weight.

The efficiency of transfer based on a distance distribution histogram can be calculated using Eq. (11). Since the histogram is already divided into N narrow intervals (Δr = 0.1 Å was used to accumulate the histogram), it is convenient to calculate the integral as a sum

$$E_{cR_0} = \sum_{i=1}^{N} P[(i-1)\Delta r < r < i\Delta r] \left\{\frac{R_0^6}{R_0^6 + [(i-\frac{1}{2})\Delta r]^6}\right\}\Delta r \quad (15)$$

where i indicates the interval number.

We note that our procedure is distinct and more complete than that used by Valeur *et al.* [13]. In this paper the authors calculated the distance distributions but evaluated the transfer efficiency for a single D–A pair with a single value of R_0. Consequently, their data did not contain information on the distribution, but only on the r^6–weighted average of the distribution.

MATERIALS AND METHODS

Each D–A pair consists of an alkyl chain linker with a tryptamine donor attached to one end and 1 of 13 acceptors attached to the opposite end. See Table I for a list of the D–A pairs and Fig. 1 for their respective structures. In general, acceptors were first attached to the linker molecule, 11–aminoundecanoic acid or its methyl ester derivative, followed by attachment of the tryptamine donor. In order to reduce the number of synthesis steps, compounds **10** and **11** were synthesized by attachment of tryptamine to 3-perylenedodecanoic acid (Molecular Probes, Eugene, OR) and 11-(9-anthroyloxy)undecanoic acid (Molecular Probes), respectively. Details of the D–A pair syntheses are given below. The compound used for donor-alone measurements is *N*-myristoyl tryptamine (TMA); its synthesis has been described previously [5]. All chemical reagents were obtained from Aldrich Chemical Co. (Milwaukee, WI) unless otherwise indicated.

Attachment of Acceptor to the Linker

Compounds 1–4 and 9

A methyl ester derivative of the linker was synthesized in order to protect its carboxylic group during the coupling of its amino group with the acceptor molecule. For synthesis of 11-aminoundecanoic acid methyl ester *p*-toluenesulfonate [14], 10 mmol 11-aminoundecanoic acid was suspended in 50 ml anhydrous methanol and then 20 mmol *p*-toluenesulfonic acid monohydrate was added. The solution was refluxed for 24 h and the alcohol was then removed under vacuum. The residue was dissolved in a minimum amount of dry methanol and crystallized with dry ether. The crystalline methyl ester *p*-toluenesulfonate 11-aminoundecanoic acid derivative was collected on a filter, washed with dry ether, and dried under vacuum over NaOH pellets. The product was used for attachment to acceptors without further purification.

Levulinyl chloride (acceptor **1**) was synthesized using

Table I. Maximum Donor–Acceptor Separations (R_{max}), Förster Distances (R_0), and Transfer Efficiencies (E_T) for the Different D–A pairs

		R_{max} (Å)[a]	R_0 (Å)	E_T
Donor alone		—	—	0.000
TMA (*N*-myristoyl tryptamide)[b]				
D–A pairs				
1.	*N*-(11-Levulinylaminoundecanoyl) tryptamide	25.5	6.26	0.080
2.	*N*-[11-(3-Acetylbenzenesulfonyl) aminoundecanoyl] tryptamide	24.2	10.4	0.280
3.	*N*-(11-Thioacetylaminoundecanoyl) tryptamide	22.3	12.6	0.400
4.	*N*-[11-(2-Ketobutyryl) aminoundecanoyl] tryptamide	23.0	13.1	0.478
5.	*N*-[11-(3-Nitrobenzenesulfonyl) aminoundecanoyl] tryptamide	24.5	13.8	0.482
6.	*N*[11-(3-Nitrobenzoyl) aminoundecanoyl] tryptamide	24.1	15.0	0.567
7.	*N*-[11-(4-Nitrobenzenesulfonyl) aminoundecanoyl] tryptamide	24.2	16.1	0.635
8.	*N*-[11-(4-Nitrobenzoyl) aminoundecanoyl] tryptamide	24.1	16.8	0.664
9.	*N*-[11-(*N*-Tosyl-3-nitrotyrosyl) aminoundecanoyl] tryptamide	25.6	24.2	0.923
10.	*N*-(3-Perylenedodecanoyl) tryptamide	24.7	26.9	0.951
11.	*N*-[11-(9-Anthroyloxy) undecanoyl] tryptamide	24.1	27.3	0.963
12.	*N*-[11-(2-Nitrobenzenesulfenyl) aminoundecanoyl] tryptamide	24.9	30.1	0.980
13.	*N*-[11-(2,4-Dinitrobenzenesulfonyl) aminoundecanoyl] tryptamide	24.2	32.7	1.000

[a] R_{max} is the energy-minimized all-*trans* separation between the donor and the acceptor. See Materials and Methods for details of the calculations.
[b] TMA was used as the donor-only molecule for all R_0 and E_T calculations.

levulinic acid and a 10% excess of thionyl chloride. For synthesis of 11-levulinylaminoundecanoic acid methyl ester, 4.1 mmol 11-aminoundecanoic acid methyl ester *p*-toluenesulfonate was dissolved in a mixture of 2.3 ml 2 *N* NaOH, 2 ml water, and 5.5 ml acetone. Simultaneously added to this mixture, in 10 equal portions, was 4 mmol levulinyl chloride dissolved in 4 ml acetone and the dropwise addition of 2.2 ml 2 *N* NaOH over a period of about 15 min. The mixture was then diluted with water, acidified with 1 *N* HCl to pH 7, and extracted with ethyl acetate. The organic phase was washed with water until the washes were neutral to Congo paper, dried over anhydrous $MgSO_4$, filtered, and then rotoevaporated. The resulting residue was purified by thin-layer chromatography (TLC) on a preparative silica gel plate. The above method was also used to synthesize and attach 2-ketobutyryl chloride (acceptor **4**) to the methyl ester derivative and for protection of the amino group of 3-nitrotyrosine (acceptor **9**) with tosyl chloride.

For synthesis of the 11-(*N*-tosyl-3-nitrotyrosyl)undecanoic acid methyl ester derivative, 5 mmol 11-aminoundecanoic acid methyl ester *p*-toluenesulfonate, 0.5 mmol triethylamine, and 5.5 mmol *N*-tosyl-3-nitrotyrosine were added to 5 ml dry chloroform. To this solution was added 5.5 mmol *N,N*-dicyclohexylcarbodiimide (DCC). The reaction mixture was stirred for 2 h, the urea by-product filtered off, and the solvent removed under vacuum. The residue was dissolved in ethyl acetate and washed three times each with 1 *N* HCl, 0.5 N $NaHCO_3$, and NaCl-saturated water. The ethyl acetate layer was dried over anhydrous $MgSO_4$, filtered, and rotoevaporated to dryness. The product was used without further purification. This method was also used to synthesize the 11-acetylaminoundecanoic acid methyl ester derivative (using acetic acid), which is subsequently used to synthesize the thioamide derivative (acceptor **3**).

To synthesize 11-thioacetylaminoundecanoic acid methyl ester, the oxygen atom in the 11-acetylaminoundecanoic acid methyl ester derivative was exchanged with sulfur by the methods of Clausen *et al.* [15,16] and Brown

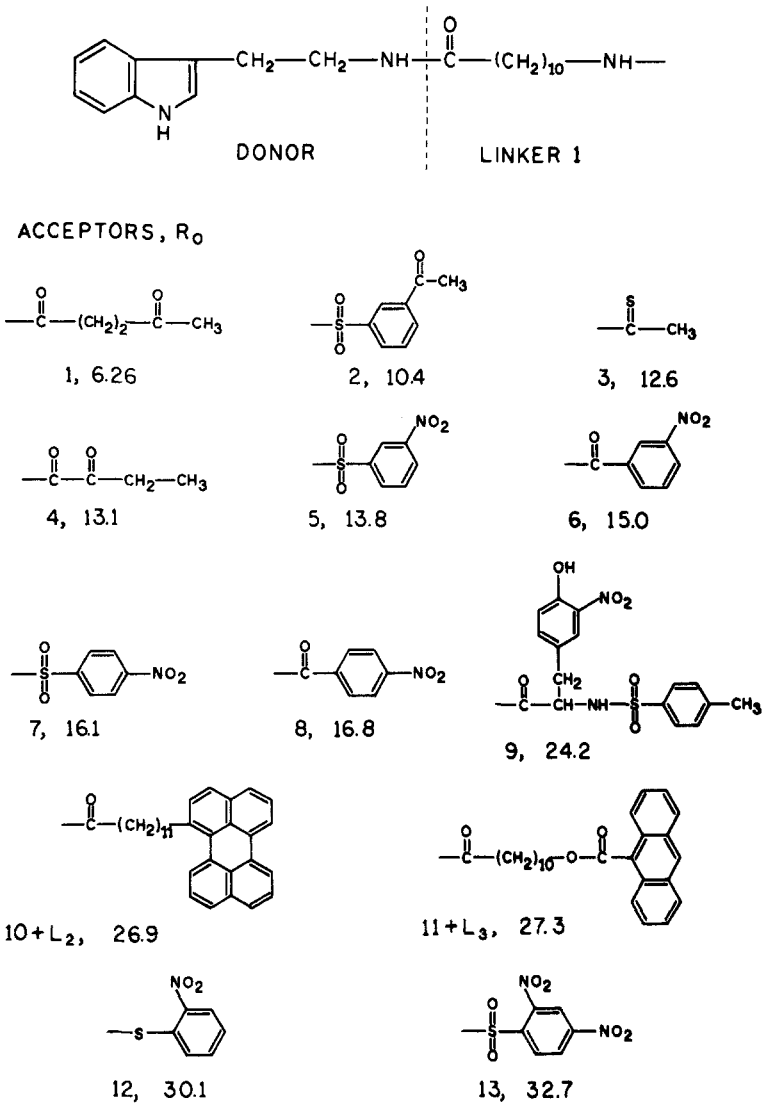

Fig. 1. Chemical structures of D–A pairs. See Table I for the chemical name which corresponds to each number. Each D–A pair consists of tryptamine attached to 11-aminoundecanoic acid (donor + linker 1) and one of the acceptors shown, except numbers 10 and 11, which contain tryptamine attached to the linkers (L_2 and L_3) shown. Following each acceptor number is the R_0 value (Å) for the corresponding D–A pair.

et al. [17]. A mixture of 1 mmol 11-acetylaminoundecanoic acid methyl ester and 0.5 mmol Lawesson reagent in 100 ml anhydrous benzene was reacted at 80°C for 4 h. The solvent was removed under vacuum and the residue was chromatographed on a silica gel preparative TLC plate followed by HPLC purification on a C_{18} column using a methanol/water mixture as eluent. For synthesis of the 11-(3-acetylbenzenesulfonyl) aminoundecanoic acid methyl ester derivative, 2 mmol 3-acetylbenzenesulfonyl fluoride (acceptor **2**), 2.2 mmol 11-aminoundecanoic acid methyl ester *p*-toluenesulfonate, and 2.2 mmol diisopropylethylamine were added to dioxane. The mixture was refluxed for 8 h and the solvent rotoevaporated. The residue was dissolved in ethyl acetate and washed three time each with 1 *N* HCl, 1 *N* $NaHCO_3$, and NaCl-saturated water. The organic phase was dried over anhydrous $MgSO_4$, filtered, and purified by chromatography on a silica gel preparative TLC plate followed by HPLC on a C_{18} column with a methanol/water mixture as eluent.

All *N*-substituted aminoundecanoic acid methyl ester derivatives were hydrolyzed before reaction with the donor molecule tryptamine. A solution of 5 mmol *N*-substituted aminoundecanoic acid methyl ester in 10 ml

methanol was put in a room-temperature water bath and 11 ml 1 *N* NaOH was added with stirring. The mixture was reacted at room temperature for 2 h and then diluted with 5 ml 1 *N* HCl. The methanol was removed under vacuum and ethyl acetate was added to the resulting aqueous solution. The organic layer was washed with water until the washes were neutral to Congo paper. The organic phase was dried over anhydrous $MgSO_4$ and the solvent removed under vacuum. The *N*-substituted aminoundecanoic acids were reacted with tryptamine without further purification.

Compounds 5–8, 12, and 13

For synthesis of 11-(3-nitrobenzenesulfonyl)aminoundecanoic acid [18], 4.1 mmol 11-aminoundecanoic acid was dissolved in a mixture of 2.3 ml 2 *N* NaOH, 2 ml water, and 5.5 ml acetone. Simultaneously added to this mixture in 10 equal portions was 4 mmol 3-nitrobenzenesulfonyl chloride (acceptor **5**) dissolved in 4 ml acetone, followed by dropwise addition of 2.2 ml 2 *N* NaOH over a period of 15 min. The mixture was then diluted with water, acidified with 1 *N* HCl, and extracted with ethyl acetate. The organic phase was washed with water until the washes were neutral to Congo paper, dried over anhydrous $MgSO_4$, filtered, and then rotoevaporated. The resulting residue was purified by TLC on a preparative silica gel plate. This same method was used for synthesis of 3-nitrobenzoyl (acceptor **6**), 4-nitrobenzenesulfonyl (acceptor **7**), 4-nitrobenzoyl (acceptor **8**), 2-nitrobenzenesulfenyl (acceptor **12**), and 2,4-dinitrobenzenesulfonyl (acceptor **13**) aminoundecanoic acids.

Attachment of Tryptamine Donor

Compounds 1–9, 12, and 13

The tryptamine donor was attached by dissolving 3 mmol of the undecanoic acid derivative, 3 mmol of tryptamine, and 3 mmol of benzotriazol-1-yloxytris-(dimethylamino)phosphonium hexafluorophosphate (BOP) in dimethylformamide/acetonitrile (1:2), followed by the addition of 9 mmol of diisopropylethylamine. The reaction mixture was stirred at room temperature for 2 h and the acetonitrile was removed under vacuum. The remaining aqueous mixture was diluted with ethyl acetate and the organic phase was washed three times each with 1 *N* HCl, 0.5 *N* $NaHCO_3$, and NaCl-saturated water. The organic layer was then dried over anhydrous $MgSO_4$, filtered, and rotoevaporated. The residue was dissolved in a small amount of ethanol and chromatographed on a silica gel preparative TLC plate, followed by HPLC purification on a C_{18} column with a methanol/water mixture as eluent.

Compounds 10 and 11

For synthesis of *N*[11-(9-anthroyloxy)undecanoyl] tryptamide, 0.22 mmol tryptamine followed by 0.22 mmol DCC was added to a solution of 0.2 mmol 11-(9-anthroyloxy)undecanoic acid (Molecular Probes) in 1 ml chloroform. The solution was stirred overnight at room temperature and the precipitated urea was removed by filtration. The filtrate was washed successively with 0.5 *N* HCl, 5% $NaHCO_3$, and NaCl-saturated water and then dried over anhydrous $MgSO_4$. The solvent was rotoevaporated and the residue was purified on a silica gel preparative TLC plate followed by HPLC purification on a C_{18} column with methanol as eluent. The same procedure was used for synthesis of *N*-(3-perylenedodecanoyl)tryptamide using 3-perylenedodecanoic acid (Molecular Probes); acetonitrile/2-propanol (1:2) was used as the HPLC eluent.

Fluorescence Measurements

All D–A pair compounds were purified by HPLC just prior to preparation of the samples for measurement. The D–A pair compounds were measured in propylene glycol at 20°C. The optical densities were near 0.1 or lower at the excitation wavelength. Emission spectra were recorded on a SLM 8000 photon counting fluorometer. Blank emission spectra were also recorded and indicated the absence of signals due to solvent impurities. Quantum yields of the donor were measured relative to a value of 0.13 for tryptophan in water at 20°C using a refractive index of 1.4324 for propylene glycol [19]. The quantum yield obtained for TMA was 0.44. The orientation factor was assumed to be 2/3, the value for a dynamically averaged random orientation. All intensities of donor–acceptor data were corrected for absorption of incident light by the acceptor using the equation of Demas and Adamson [20]; in our case the quencher is the acceptor.

R_{max} Calculations

Maximum separation between the donor and the acceptor (R_{max}) in the D–A pair compounds was calculated using the molecular graphics/dynamics programs QUANTA (Version 2.1A) and CHARMm (Polygen Corp., Waltham, MA). The distances are approximated using the energy-minimized all-*trans* conformation. The

point of measurement in the donor was the middle of the bicyclic indole bond. The point of measurement in the acceptors was in the middle of the double bond farthest away from the donor (compounds **1, 3,** and **4**), the center of the relevant six-membered ring, or the center of the central six-membered ring when more than one is present.

RESULTS

Experimental Distance Distributions

Table I lists the maximum donor–acceptor separations (R_{max}), Förster distances (R_0), and energy transfer efficiencies (E_T) for each D–A pair compound. All 13 D–A pairs (Fig. 1, Table I) contain a tryptamine donor at one end of a flexible alkyl chain linker and a different acceptor attached at the opposite end. The alkyl chain linker is approximately the same length in all the D–A pair compounds; the range of R_{max} values is 23.0–25.6 Å (Table I). Hence, the end-to-end distance distribution should be the same for all these D–A pairs. The range of R_0 values for the 13 D–A pair compounds is 6.26–32.7 Å, which is a good range for recovering the steady-state distance distribution from our chosen linker molecule (average R_{max} = 24.3 Å). Previous studies [4,5] on a D–A pair with this same linker revealed an average distance of 12–13.5 Å and a half-width of 12–15 Å, which suggests that the present series of D–A pairs can sample the entire range of accessible distances. The steady-state emission spectra for the donor alone molecule (TMA) and 12 of the 13 D–A pairs are shown in Fig. 2. All the D–A pairs were measured in propylene glycol so that end-to-end diffusion could be excluded from the distance distribution calculations. More specifically, we recently used the frequency-domain data to measure the end-to-end diffusion coefficient of similar molecules [21]. At 20°C in propylene glycol, diffusion did not significantly affect the apparent distance distribution recovered with a tryptophan donor [22]. The emission spectrum for D–A pair 4 depicted in Fig. 2 is also representative of D–A pair 5 since its spectrum is nearly equivalent. The emission of D–A pairs 10 and 11 have fluorescent acceptors. As expected, the donor emission is increasingly quenched by the acceptor as the R_0 increases.

Figure 3 shows a plot of E_T versus R_0, which are the data used to recover the distance distribution from the steady-state measurements. One notices that as R_0 increases, the transfer efficiency increases from 0 (no acceptor) to 100%. These data were used in our nonlinear least-squares fitting algorithm to recover the end-to-

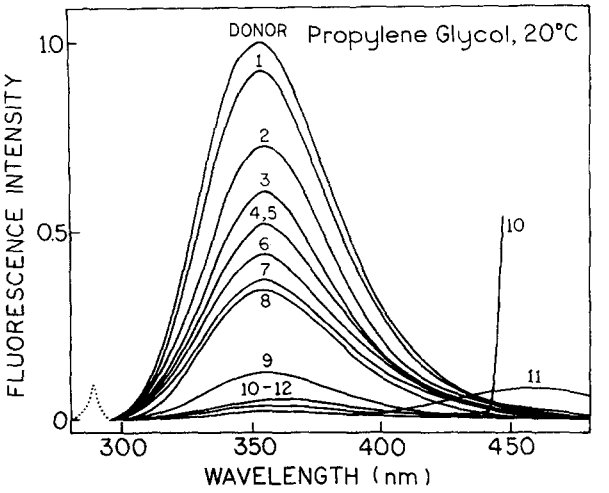

Fig. 2. Emission spectra of the donor alone (TMA) and the D–A pairs. See Table I for identification of each number. All D–A pairs were measured in propylene glycol at 20°C with an excitation wavelength of 290 nm. Spectra 4 and 5 were nearly equivalent; the former is shown and is representative of both D–A pairs. The spectrum of compound **13** is completely quenched and is thus not shown.

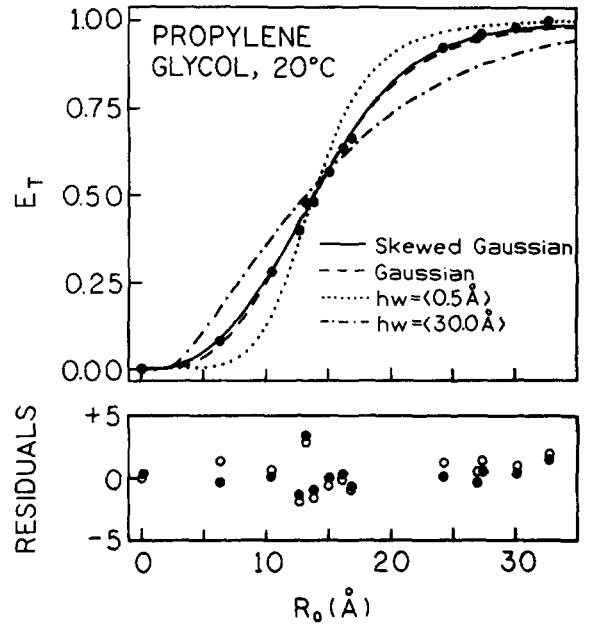

Fig. 3. Plot of the measured energy transfer efficiencies (E_T) versus the Förster distance (R_0) for the 13 D–A pairs listed in Table I. The data are fit with a Gaussian model (– – –) and a skewed Gaussian model (——). Calculated curves for a fixed narrow distribution (• • •) and a fixed wide distribution (— • —) are also shown.

end distribution. As can be seen from the close overlap of the data and the theoretical curves, both the Gaussian (– – –) and the skewed Gaussian (—) models appear to fit the transfer efficiency data quite well. We tried to fit the data with a Gaussian model in which the half-width of the distribution (*hw*; full width of the distribution at half-maximum) is fixed with either a narrow (*hw* = ⟨0.5⟩ Å) or a wide (*hw* = ⟨30.0⟩ Å) distribution; however, this resulted in large deviations between the calculated curves and the data points (Fig. 3). The inability to fit the data with a narrow distribution indicates that the molecules are not in some fixed conformation with a unique distance between the donor and the acceptor. The inability to fit the data to a fixed wide distribution (*hw* = ⟨30⟩ Å) demonstrates that the data are not consistent with such a wide distribution and suggests that the data contain significant information on the width of the distribution. The steady-state distance distribution parameters resulting in the best fit to the data are listed in Table II. Despite the reasonably good fit to the Gaussian model, it appears that the skewed Gaussian fit is superior as evidenced by its lower χ_R^2 value (Table II).

Upon visual inspection of the data points Fig. 3, we noticed that the fifth data point (representing D–A pair 4) does not appear to follow the smooth line of the calculated curve and, thus , probably was measured with some amount of error. Therefore, we decided to reanalyze the data with omission of the transfer efficiency for D–A pair 4. This resulted in a significant improvement in the analyses (Table II) as evidenced by the lower χ_R^2 values for both the Gaussian and the skewed Gaussian models. More importantly, the skewed Gaussian has a threefold lower χ_R^2 value than the Gaussian and thus more convincingly indicates the presence of a skewed Gaussian distribution.

The distance distribution curves recovered with both the Gaussian and the skewed Gaussian models are shown in Fig. 4 (top). The skewed Gaussian model has the additional parameter *s*, which describes the degree of skewness in the curve ($s = 0$ for the Gaussian model). For the Gaussian curve, $\bar{r}$ is the mean of the distribution and represents the most populated conformational state for the molecule. The analogous parameter for the skewed Gaussian curve is r_m, which is the most frequently occurring value of the distribution [9]. The distance distributions allowable within the 67% confidence interval are also shown in Fig. 4 (bottom), with the maximum range being given by the shaded area. We note that this range of distributions was obtained with consideration of correlation between the parameters, as described below (Fig. 5). Hence, based on this figure, the skewed end-to-end distribution is determined with good confidence by our data.

The major difference between the Gaussian and the skewed Gaussian curves is the D–A pair distance which represents the most populated conformation of the mol-

Table II. Distance Distributions from the Steady-State Data Using Gaussian and Skewed Gaussian Models

Model	$\bar{r}$ or r_m (Å)[a]	*hw* (Å)[b]	*s*[c]	χ_R^2	F_x[d]	*P*[e]
Gaussian	14.07	11.32	⟨0.00⟩	2.18		
	13.93	⟨0.5⟩	⟨0.00⟩	36.6		
	7.38	⟨30.0⟩	⟨0.00⟩	46.7		
Skewed Gaussian	18.36	11.28	−1.57	1.61	4.41	0.068
Gaussian[f]	14.15	11.13	⟨0.00⟩	1.52		
Skewed Gaussian[f]	18.73	10.84	−1.79	0.49	19.6	0.0024

[a] $\bar{r}$ is the mean of the distance distribution for the Gaussian model and r_m is the most frequently occurring value for the skewed Gaussian model.

[b] *hw* is the full width of the distribution at half-maximum; ⟨0.5⟩ and ⟨30.0⟩ indicate fixed narrow and wide distributions, respectively, during the least-square fitting procedure. The half-width (*hw*) is proportional to the standard deviation (σ) referred to under Theory: $hw = 2.354\sigma$.

[c] *s* is the skew parameter, which indicates the degree and direction (negative or positive) of skewness for the distribution curve; $s = 0$ for a nonskewed Gaussian curve.

[d] $F_x = (\chi^2_{Gau} - \chi^2_{xGau})/[\chi^2_{sGau}/(N-n)]$; $N = 13$ or 12, $n = 3$[27].

[e] Probability that this F_x ratio is due to random error in the data[27].

[f] These two sets of analyses were performed omitting the transfer efficiency for D–A pair 4.

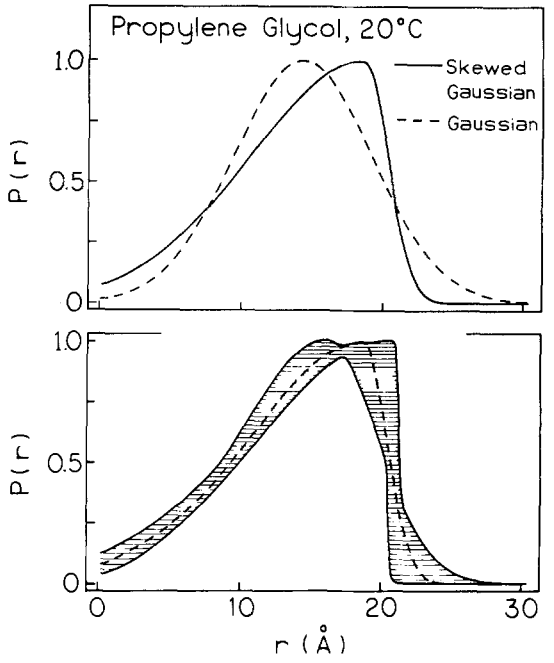

Fig. 4. Top: Distance distribution curves recovered from steady-state measurements on the 13 D–A pairs. Both Gaussian (– – –) and skewed Gaussian (——) curves are shown. See Table II for the parameters which describe each model. Bottom: The degree of uncertainty in the skewed Gaussian distribution; the shaded area represents the 67% confidence interval.

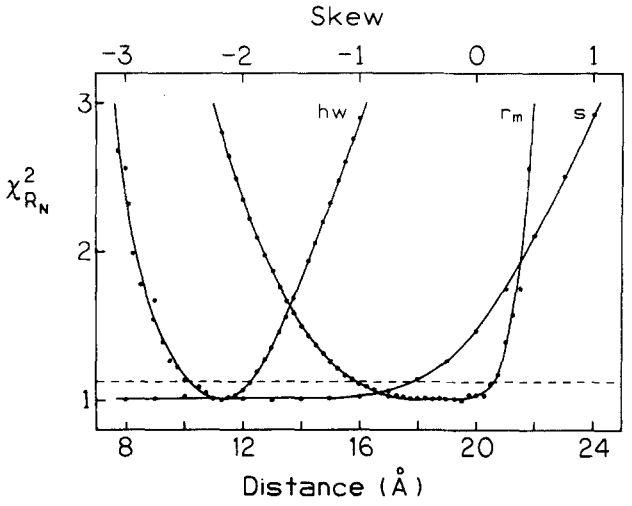

Fig. 5. Normalized χ^2_R surfaces for the skewed Gaussian model parameters (*hw*, r_m, and *s*). The units (Å) for the *hw* and r_m are shown at the bottom; *s* is a unitless parameter whose numerical quantity, shown at the top, indicates the degree and direction (positive or negative) of the skew. The dashed line indicates the 67% confidence intervals for $F(1,10)$. The ratio χ^2_R (two parameters floated) over χ^2_R (three parameters floated) is directly related to F_χ: $F_\chi = [(N - 2)(\chi^2_{R,2\ param}/\chi^2_{R,3\ param})] / (N - 3)$.

ecule, $\bar{r}$ and r_m (Table II). In the skewed Gaussian curve the maximum D–A pair distance is ~23 Å, whereas in the Gaussian curve the maximum distance almost extends to the maximum value specified in the analysis program (30 Å). This is consistent with the dimensions of the D–A pair compounds which have an average calculated R_{max} of 24.3 Å and, thus, would not be able to access conformations much greater than this value.

The merit of the additional skew parameter between the Gaussian and the skewed Gaussian models was evaluated using the F_χ statistic for the ratio of independent reduced chi-square [27]. The difference between the unreduced two- and the unreduced three-parameter χ^2 values is independent of χ^2_{sGau} and distributed with one degree of freedom. In this case F_χ is the reduced chi-square ratio, $(\chi^2_{difference}/1) \div [\chi^2_{sGau}/(N-n)]$, where N is the number of data points (13, or 12 if point 4 is excluded), n is the number of fitted parameters (i.e., 3), and $\chi^2_{difference} = \chi^2_{Gau} - \chi^2_{sGau}$. The *P*- values associated with this F_χ ratio were determined from tabulated $F[\nu_1 = 1, \nu_2 = 10$ (or 9)] distribution functions [27]. The value of 0.062 is close to the usual 0.05 threshold for significance; after the outlying data point, number 4, was removed, this *P* value declined to 0.0024.

It is of importance to consider the confidence interval of the parameters which describe the distance distribution or, equivalently, the range of distance distributions which are consistent with our experimental data. This was done for the skewed Gaussian distribution and was accomplished by examination of the χ^2_R surfaces for the parameters describing the distributions, r_m, *hw*, and *s*. To constrain these surfaces we held one parameter at a fixed value and minimized χ^2_R by adjustment of the remaining parameters. This procedure accounts for correlation between the parameters. These χ^2_R surfaces are shown in Fig. 5. One notices that the parameters r_m and *hw* are determined to small limits by our data. However, χ^2_R surface of the skewness parameters shows a much wider range of possible parameter values. Despite this degree of variation, these parameters do not result in remarkably different distance distributions (Fig. 4, bottom). More specifically, the negative value of *s* is not constrained by the experimental data. However, increasingly negative values of *s* result in a more sharply defined maximum distance, as seen in Fig. 4.

Comparison with Theoretical Distance Distributions

These experimental distance distributions are suitable for comparison with the predictions based on the

statistics of chain molecules [2]. We calculated the end-to-end distance distributions for these 13 molecules, using the models for a freely jointed chain (FJ), a freely rotating chain (FR), a rotationally restricted chain (RR), and the rotational isomeric state model (RIS). Only 1 of the 13 D–A pair molecules was simulated since the model is, in principle, uniformative about the behavior within the end groups (donor and acceptor) and assignment of different parameters to describe the energy potentials within them would be essentially arbitrary.

The geometric and energetic parameters used are given in Table III. Refer to Fig. 6 for the bond numbers. The polyamide bond energies described by Flory [2] are used for the alkyl bonds and the first and second bonds preceding the amide and the sulfonamide bonds. Typical values for an alkyl chain are about 0.5 kcal/mol for any *gauche* bond and about 2 kcal/mol if a *gauche*$^+$ bond occurs adjacent to a *gauche*$^-$ one. The parameters for the three bonds following the amide or sulfonamide are based on those for the first [23], second [24], and third [25] bonds following an ester linkage [26]. The rotational positions of the first and last bonds in the chain are not weighted with respect to rotational position.

Since the number of conformations in this set is very high, a Monte Carlo sampling method was used to generate a representative sample [11,12]. The histograms representing the different models are shown in Fig. 7. They were accumulated using 0.1-Å intervals and their shapes are smoothed out by displaying them with 0.5-Å intervals. In practice it was found that since the rotational restrictions were in each case totally symmetric, the resulting distance distribution histograms for the RR and FR models were essentially identical. Only the latter is depicted in Fig. 7.

In a comparison of the distance distribution histograms of the various models (Fig. 7), it is evident that those representing the freely jointed chain (FJ) and freely rotating chain (FR) models are inconsistent with the parameterized curve based on the data, whereas the rotational isomeric state (RIS) model histogram closely matches the data-fitted skewed Gaussian distribution. The experimental data support the RIS model and provide the capability for refining the parameters which describe the statistical mechanics of chain molecules.

The distance distribution histograms for the different models were used to simulate steady-state energy transfer data. These simulated data curves are shown in Fig. 8, as well as the experimental data points from Fig. 3. Again, it is evident that the freely jointed chain and freely rotating chain models are inconsistent with the

Table III. Survey of Input Parameters for the RIS Model[a]

	Bond geometry[c]			Bond energy[e]	
Bond no.[b]	Length (Å)	Angle (degrees)	Rotational position[d]	E_σ (cal/mol)	E_ω (cal/mol)
1	1.85	—	—	0	0
2	1.82	120	2	0	0
3	1.62	109.5	3	0	0
4	1.46	109.5	3	0	0
5	1.53	112	3	0	1360
6	1.54	112	3	0	1360
7–11	1.54	112	3	498	1995
12	1.54	112	3	498	556
13	1.51	112	3	−200	∞
14	2.38	142.6	3	397	0
15	1.46	158.4	3	0	0
16	1.53	112	3	0	1360
17	1.54	112	3	0	1360
18	1.56	152.6	2	0	0

[a] The input parameters were derived from *N*-[11-(dansyl)aminoundecanoyl] tryptamide. The simulation temperature was 300 K.

[b] Numbered bonds are shown in Fig. 6.

[c] Sources include Ref. 2, pp. 145–146; Ref. 28; and Ref. 29.

[d] 2 = rotational positions 0 and 180°; 3 = rotational positions 0° (*trans*), 120° (*gauche*$^+$), and −120° (*gauche*$^-$).

[e] These are approximate energy values, where E_σ denotes the energy cost for a *gauche* bond and E_ω denotes the additional cost of a *gauche*$^+$/*gauche*$^-$ interaction.

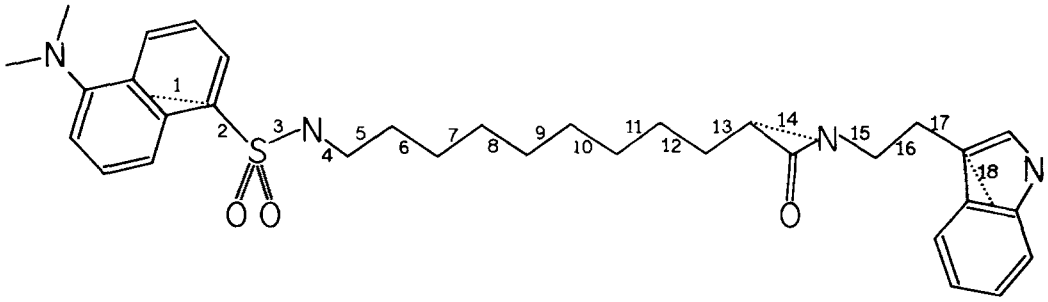

Fig. 6. Molecule (*N*-[11-(dansyl) aminoundecanoyl] tryptamide) used for the distance distribution simulations. All atoms are carbon unless otherwise indicated; hydrogen atoms are not shown. Bonds are numbered 1–18; the geometric and energetic parameters for each bond are given in Table III. Bonds 7–11 are equivalent; 1, 14 (the peptide bond is *trans*), and 18 are virtual bonds (• • •), which span more than one bond [2].

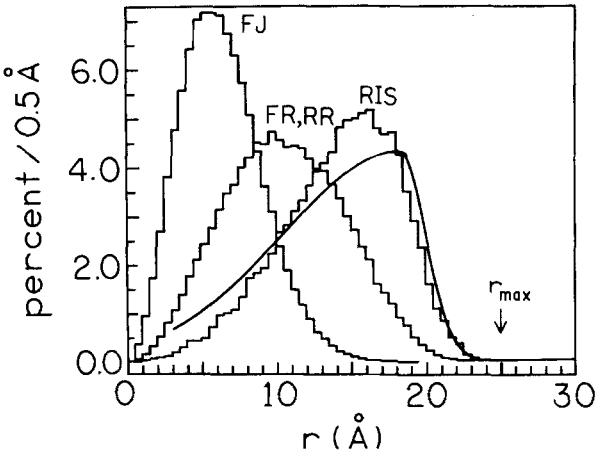

Fig. 7. Comparison of distance distribution histograms predicted with the rotational isomeric state (RIS), freely rotating (FR), and freely jointed (FJ) models with the steady-state fitted curve (smooth line). The freely rotating (FR) histogram is also representative of the rotationally restricted (RR) model. The arrow indicates the average R_{max} value (24.3 Å). See Table II for the parameters describing the steady-state skewed Gaussian distribution curve.

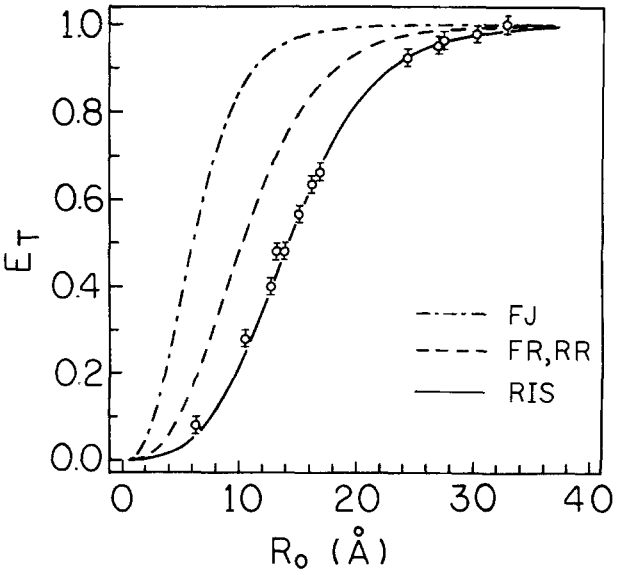

Fig. 8. Comparison of the simulated data curves calculated from the histograms shown in Fig. 7 to the experimentally measured data (points). The simulated curves represent the rotational isomeric state (RIS), freely rotating (FR) and rotationally restricted (RR), and freely jointed (FJ) models.

steady-state data set since their curves are significantly shifted to higher amounts of energy transfer. Conversely, the RIS model curve closely approximates the steady-state data set. The slight overestimate in transfer efficiency seen in the RIS model curve could be due to a variety of inaccuracies in the experimental data or the energetic or conformational parameters chosen to describe the molecules.

DISCUSSION

We have verified Cantor and Pechukas' method for recovering end-to-end distance distributions from steady-state energy transfer measurements on D–A pairs with different R_0 values. The transfer efficiency data plotted as a function of R_0 were fit with both Gaussian and skewed Gaussian models. The distribution recovered with the skewed Gaussian model has a twofold lower χ^2_R value than the distribution obtained with a Gaussian model. Thus, we conclude that the skewed Gaussian model is a more accurate description of the end-to-end distance distribution for these flexible molecules. We believe that this is the first report of an experimentally determined

skewed Gaussian distribution. Additionally, our experimental data are consistent with simulated data based on the rotational isomeric states model, which predicts a skewed, unimodal distribution for these molecules.

The methods and analysis described in this paper allow the comparison of experimentally determined conformational distributions of molecules with those predicted from theory. The latter predictions are dependent upon the model and the steric, electrostatic, and bonding parameters which it contains. Consequently, it is now possible to test and/or refine such models by comparison with experimental results. Such comparisons are of considerable interest to biochemistry and biophysics, where it is desirable to predict the conformation of proteins and nucleic acids based on primary structure.

APPENDIX: EXPLANATION OF THE DISTANCE DISTRIBUTION FUNCTION *P(r)*

In his classic work Flory [2] discusses the theoretical distance distribution function for infinite chains with various conformational constraints. However, to the best of our knowledge, expressions do not exist to describe the end-to-end distributions of the finite-length molecules described in the report. Hence, we arbitrarily chose the one-dimensional Gaussian distribution [Eq. (5)]. To avoid confusion it seems appropriate to describe the relationship between our empirical model and Flory's molecular model.

As Flory [2] discusses, for large n a freely jointed homopolymeric chain, which does not interact with itself, is equivalent to a random walk in space. If one puts the first end at the origin and considers the end-to-end vector, **r**, then for large values of n the probability density function describing the probability of finding the other end within volume element dv at position r is given by

$$W(\mathbf{r})dv \sim A\exp\left(-\frac{|\mathbf{r}|^2}{B}\right) = A\exp\left(-\frac{r^2}{B}\right) \quad \text{(A1)}$$

(A and B are appropriate constants). Since for large n the probability density is approximately spherically symmetric, the probability of finding the other end within the volume element may be determined by integrating over the spherical shell defined by $r \le |\mathbf{r}| \le r + dr$. Hence, our $P(r)$ is related to Flory's $W(r)$ by

$$P(r)dr = \int_{r\le|\mathbf{r}|\le r+dr} W(\mathbf{r})dv$$

$$= 4\pi r^2 A\exp\left(-\frac{r^2}{B}\right)dr \quad \text{(A2)}$$

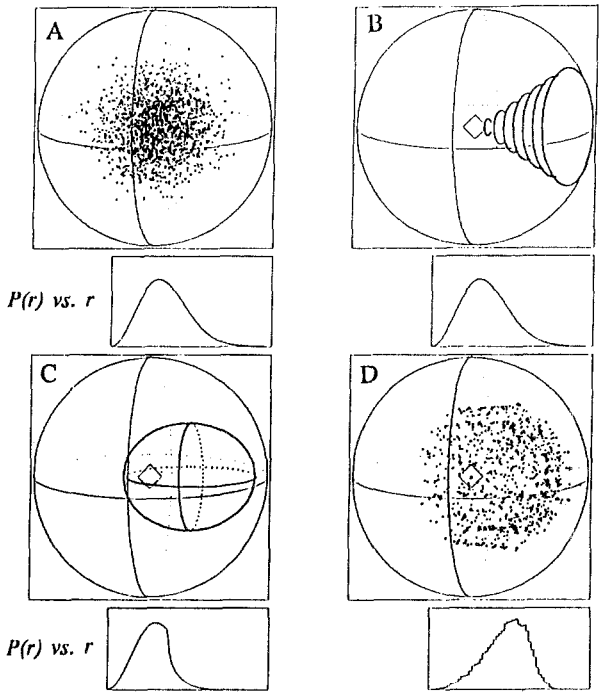

Fig. 9. Distance distribution for various constraints on the allowed volume for the acceptor. See Appendix for additional detail.

The new constant terms can be absorbed into the preexponential factor to emphasize that the net change is the addition of the r^2 factor.

$$P(r)dr = A'r^2\exp\left(-\frac{r^2}{B}\right)dr \quad \text{(A3)}$$

In a previous report [5] we demonstrated that the shape of the end-to-end distribution was not affected by the use of r^2 in the distribution functions. Of course, the parameter describing the distribution functions were different, but the overall shape was unchanged.

In the present report we are dealing with donor and acceptors linked by a finite-length spacer. This results in at least two difficulties in selecting the distribution function. First, the mean D–A distance will be nonzero because of the finite size of the donor and acceptor and because of steric constraints imposed by the finite-length linker. Second, not all the three-dimensional space is available to the acceptor. The latter point is clarified by recalling that the linker is initially directed away from the donor in a single direction. There exists the probability that the spatial distribution is not radially symmetric about the origin. Based upon these considerations we are required to allow for a

nonzero mean, and the choice of a volume element [$4\pi r^2 dr$ in Eq. (A2)] is not clear.

Conceding that these alterations (the probability density function is not centered at the origin and is not radially symmetric) are superimposed on the Gaussian density function describing the limit (as $n \rightarrow$ infinity) of the end-to-end distribution function for a freely jointed chain, we arrive at the two-parameter probability distribution fitting function described in the paper ($B = 2\sigma^2$; Z_{Gau} is the normalization constant)

$$P(r) = \frac{1}{Z_{Gau}} \exp\left[-\frac{1}{2}\left(\frac{r - m}{\sigma}\right)^2 \right] \qquad \text{(A4)}$$

These concepts are illustrated schematically in Fig. 9. In Fig. 9A the data represent the density function $W(r)$ for the case of a freely rotating chain with $n = 100$ bonds. For clarity, only the points which are very close to the plane of the page are shown. Notice that (i) $W(r)$ is spherically symmetric, (ii) the maximum is at the mean value, and (iii) the mean position is at the origin, $r = 0$. However, when presented in terms of the distance distributions within volume elements r to $r + dr$, the $P(r)$ distribution has a Gaussian-like appearance and is no longer centered at $r = 0$.

It is easy to imagine that geometric restrictions of the linker could alter the volume accessible to the acceptor. Two such cases are shown in Figs. 9B and 9C, which show the acceptor to be restricted to a cone and an ellipsoid, respectively. Such restrictions again result in Gaussian-like $P(r)$ distributions, perhaps with somewhat greater asymmetry. And finally, Fig. 9D shows the $W(r)$ distributions for the linker described in the paper with $n = 18$ bonds. Again, only the end points in the plane of the page are shown. The distribution contrasts with that of the freely jointed chain in several ways: (i) it is not spherically symmetric (denser crescent on the right edge), (ii) the maximum density is not at the mean value (but rather somewhere on that right edge), and (iii) the mean position is displaced from the origin. The inset shows the $P(r)$ function determined from this simulation. Hence, we conclude that the Gaussian $P(r)$ distribution used in this paper provides a realistic representation of the type of distribution expected for finite-sized linkers.

ACKNOWLEDGMENTS

J.R.L. and W.W. acknowledge support from the Medical Biotechnology Center at the University of Maryland and P.E. acknowledges fellowship support from the University of Maryland Graduate School. M.F. acknowledges support from National Institutes of Health Grant GM 08181-03. This work was supported by Grant R01-GM35154 from the National Institutes of Health and Grant DMB-8502835 from the National Science Foundation.

REFERENCES

1. C. R. Cantor and P. Pechukas (1971) *Proc. Natl. Acad. Sci. USA* **68**, 2099–2101.
2. P. Flory (1969) *Statistical Mechanics of Chain Molecules*, John Wiley & Sons, New York, Chaps. 1, 3, and 5.
3. I. Gryczynski, W. Wiczk, M. L. Johnson, and J. R. Lakowicz (1988) *Chem. Phys. Lett.* **145**, 439–446.
4. I. Gryczynski, W. Wiczk, M. L. Johnson, H. C. Cheung, C.K. Wang, and J. R. Lakowicz (1988) *Biophys. J* **54**, 577–586.
5. J. R. Lakowicz, M. L. Johnson, W. Wiczk, A. Bhat, and R. F. Steiner (1987) *Chem. Phys. Lett.* **138**, 587–593.
6. J. R. Lakowicz, I. Gryczynski, H. C. Cheung, C.K. Wang, and M. L. Johnson (1988) *Biopolymers* **27**, 821–830.
7. J. R. Lakowicz, I. Gryczynski, H. C. Cheung, C.K. Wang, M. L. Johnson, and N. Joshi (1988) *Biochemistry* **27**, 9149–9159.
8. S. Albaugh and R.F. Steiner (1989) *J. Phys. Chem.* **93**, 8013–8016.
9. R. D. Remington and M. A. Schork (1985) *Statistics with Applications to the Biological and Health Sciences*, Prentice-Hall, Englewood Cliffs, NJ, Chap. 2, p. 14.
10. E. Haas, C. A. McWherter, and H. A. Scheraga (1988) *Biopolymers* **27**, 1–21.
11. N. A. Metropolis, A. W. Rosenbluth, M. N. Rosenbluth, A. H. Teller, and E. Teller (1953) *J. Chem. Phys.* **21**, 1087–1092.
12. S. Prémilat and J. Hermans Jr. (1973) *J. Chem. Phys.* **59**, 2602–2612.
13. B. Valeur, J. Mugnier, J. Pouget, J. Bourson, and F. Santi (1989) *J. Phys. Chem.* **93**, 6073–6079.
14. E. Hardin Strickland, J. Horwitz, E. Kay, L. M. Shannon, M. Wilchek, and C. Billups (1971) *Biochemistry* **10**, 2631–2638.
15. K. Clausen, M. Thorsen, and S.-O. Lawesson (1982) *Chem. Scripta* **20**, 14–18.
16. K. Clausen, M. Thorsen, and S.-O. Lawesson (1981) *Tetrahedron* **37**, 3635–3639.
17. D. W. Brown, M. M. Campbell, and C. V. Walker (1983) *Tetrahedron* **39**, 1075–1083.
18. M. Bodanszky and A. Bodanszky (1984) *The Practice of Peptide Synthesis*, Springer-Verlag, Berlin, Chap. 1A, p. 26.
19. R. F. Chen (1967) *Anal. Biochem.* **1**, 35–42.
20. J. N. Demas and A. W. Adamson (1973) *J. Am. Chem. Soc.* **95**, 5159–5168.
21. J. R. Lakowicz, J. Kusba, W. Wiczk, and I. Gryczynski (1990) *Chem. Phys. Lett.* **173**,.319–326.
22. J. R. Lakowicz *et al.*, unpublished observations.
23. A. Abe, R. C. Jernigan, and P. J. Flory (1966) *J. Am. Chem. Soc.* **88**, 631–639.
24. A. Abe and J. E. Mark (1976) *J. Am. Chem. Soc.* **98**, 6468–6476.
25. E. Riande and J. Guzman (1985) *J. Polym. Sci. Polym. Phys. Ed.* **23**, 1235–1245.
26. W. Mattice, personal communication.
27. P. R. Bevington (1969) *Data Reduction and Error Analysis for the Physical Sciences*, McGraw-Hill, New York, pp. 200–201, 318.
28. *66th Handbook of Chemistry and Physics* (1985) CRC Press, Boca Raton, FL, pp. F-165–F-166.
29. R. W. G. Wyckoff (1966) *Crystal Structures*, John Wiley & Sons, New York, pp. 53, 82, 288, 682.